crystals

MDPI

Article

Crystal Structure vs. Vibrational Behavior of Wollastonite-1*A* from Băița Bihor, Bihor Mountains, Romania

Ştefan Marincea [1,*], Delia-Georgeta Dumitraş [1], Frédéric Hatert [2], Cristina Sava Ghineț [1], George Dincă [1,3], Aurora-Măruța Iancu [1] and Martin Depret [2]

[1] Department INI, Geological Institute of Romania, 1 Caransebeş Str., RO-012271 Bucharest, Romania; d_deliaro@yahoo.com (D.-G.D.); ghinet.cristina@yahoo.com (C.S.G.); georgedinca@rocketmail.com (G.D.); iancu.maruta@yahoo.com (A.-M.I.)
[2] Laboratoire de Minéralogie, Université de Liège, Sart-Tilman, Bâtiment B 18, B-4000 Liège, Belgium; fhatert@uliege.be (F.H.); martin.depret@uliege.be (M.D.)
[3] Research Center for Ecological Services (CESEC), University of Bucharest, RO-050663 Bucharest, Romania
* Correspondence: smarincea@yahoo.com or marincea@igr.ro

Abstract

Wollastonite-1*A* from Băița Bihor occurs in distal calcic skarns developed in the contact zone of a mainly granodioritic batholith, of Upper Cretaceous age, with Mesozoic limestones and dolostones. Wollastonite generally occurs in the inner part of metasomatic columns, in monomineralic skarns or associated with grossular and molybdenite-2*H* as ore mineral. The physical properties (i.e., refraction indices α = 1.616, β = 1.629, and γ = 1.631, $2V_{\alpha}$ = 39° and density D_m = 2.922(3) g/cm^3) are typical for a term close to the stoichiometry, which is confirmed by the chemical analysis. The chemical structural formula of the analyzed wollastonite-1*A* is $(Ca_{1.000}Mg_{0.002}Mn_{0.001}Fe_{0.001})(Al_{0.004}Ti_{0.001}Si_{0.994})O_3$, which closely approximates the ideal $CaSiO_3$. The Gladstone–Dale compatibility indices account for an excellent agreement between physical and chemical data. The mineral can be satisfactorily refined as triclinic, space group $P\bar{1}$, with R_1 = 0.0678 and cell parameters a = 7.9233(3) Å, b = 7.3203(3) Å, c = 7.0651(3) Å, α = 90.053(3)°, β = 95.208(3)°, γ = 103.384(3)°. Both the IR and Raman spectra principally reveal bands related to vibrations of bridged and non-bridged oxygens pertaining to SiO_4 structural tetrahedra. At Băița Bihor, wollastonite-1*A* is part of the prograde paragenesis, marked by a peak temperature of 550–600 °C.

Keywords: wollastonite-1*A*; physical properties; crystal chemistry; single-crystal X-ray diffraction; crystal structure; infrared and Raman spectra; calcic skarns; Upper Cretaceous; Băița Bihor; Romania

Academic Editor: Shin-ichi Kimura

Received: 4 March 2026
Revised: 25 March 2026
Accepted: 30 March 2026
Published: 7 April 2026

1. Introduction

The isochemical group of minerals with ideal formula $CaSiO_3$ comprises two polymorphs, i.e., α-wollastonite (pseudowollastonite) and β-wollastonite, respectively. β-wollastonite has many polytypes recognized as mineral species (e.g., [1]), most of them triclinic (wollastonite-1*A*, -3*A*, -4*A*, -5*A*, and -7*A*, respectively) and one monoclinic (wollastonite-2*M*). The 1*A* polytype, longtime referred to as wollastonite *sensu stricto* (e.g., [2]), is by far the most abundant and common. Due to its properties (fibrous texture; white color; very low loss on ignition, which reduces gas bubble entrapment and gas dispersion during heating; thermal stability until about 1120 °C), wollastonite is a "ver-

satile" industrial mineral [3] with its main utilities as white pigment, basic compound for ceramic glazes and enamels, filler and extender for the rapidly growing polymers (rubber and plastic), substitute for asbestos, flock fibers in coatings, plasters and paintings, flux in the casting of steel, ingredient for special cements, decorative stone, and even for carbon dioxide capture (e.g., [3–8]).

Mentioned by von Zepharovich [9] and first analyzed by Loczka [10], wollastonite from Băița Bihor is one of the about 120 mineral species described so far in this huge deposit, well known for its very complex mineralogy (e.g., [11–13]). A first structural refinement, attempted using the Rietveld method, was based on very few reflections from the X-ray powder pattern and seems in error, since the authors [14] described the 2*M* polytype. In spite of the frequency of its apparition in the contact area and particularly in the calcic skarns, there remains a relative paucity of data about the composition, optics, vibrational behavior and crystallographic parameters of wollastonite from Băița Bihor as compared with the existing similar data on other mineral species from this worldwide famous occurrence.

Substantiating a preliminary evaluation for its use as industrial mineral, the present study presents a complex investigation of wollastonite-1*A* from Băița Bihor in order to offer more tools for successful processing.

2. Geological Setting

The contact–metasomatic area in Băița Bihor (also known under its old name, i.e., Rezbanya) is one of the most important in the so-called "Banatitic Magmatic and Metallogenetic Belt"—BMMB [15]. BMMB can be defined as one of the most relevant Upper Cretaceous magmatic and metallogenetic manifestations worldwide. The BMMB belt, also known as the Upper Cretaceous Apuseni–Banat–Timok–Srednogorie (ABTS) belt (e.g., [16]), represents a series of discontinuous magmatic and metallogenic occurrences of Upper Cretaceous age, which are discordant in respect to mid-Cretaceous nappe structures ([17–21] and references therein) and extend from Romania (Apuseni Mountains) to Serbia (Timok), Northern Macedonia and Bulgaria (Figure 1). The formation and evolution of the BMMB was early ascribed to subduction models involving either slab-rollback or slab-tear mechanisms affecting the subduction front of the Vardar Ocean ([19] and references therein). "Banatites" were also regarded as post-collisional type I magmatites and were ascribed the abundance of ore deposits in the eastern part of the Alpine–Balkan–Carpathian–Dinarides (ABCD) realm to a slab break-off of subducted lithosphere fragments during the Vardar Ocean closure, which imposed the rolling back and steepening of slabs [22]. This process leads to upper crust extension and favored the access of melts to high crustal levels. The Cenozoic collision between Tisia and Dacia blocks might be responsible for overall crustal thickening, for the formation of extensional faults that facilitated magma upwelling, and for a clockwise rotation of 60–80° with respect to the initial east–west trend at the time of "banatite" emplacement ([18,20,21] and references therein). A sketch of the Banatitic Magmatic and Metallogenetic Belt in the peculiar structural complex of Romania is given in Figure 1, while Figure 2 offers a simplified geological sketch of the Băița Bihor area.

https://doi.org/10.3390/cryst16040247

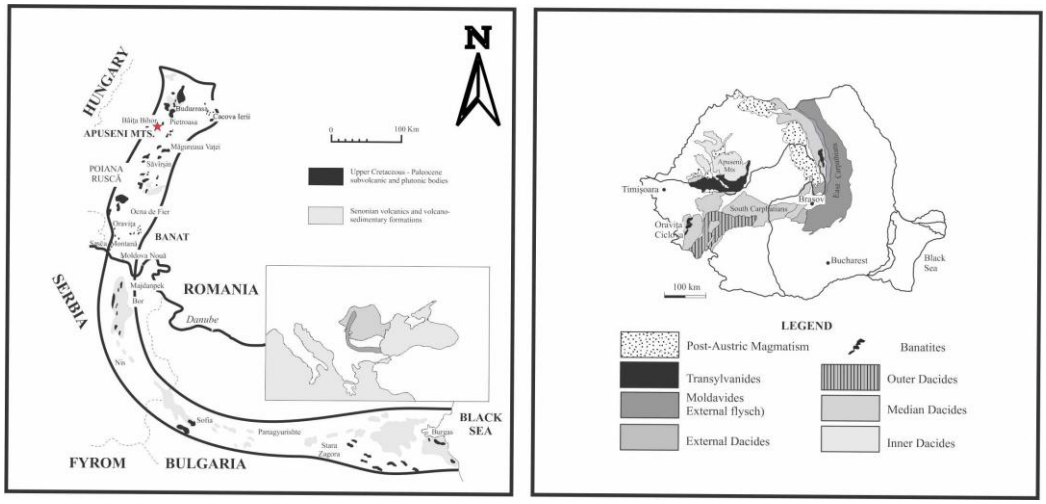

Figure 1. Sketch of the Banatitic Magmatic and Metallogenetic Belt (top, **left**: redrawn from [17]) and the structural context of Romania (top, **right**: redrawn from [23], simplified). The location of the studied occurrence is marked with a red star.

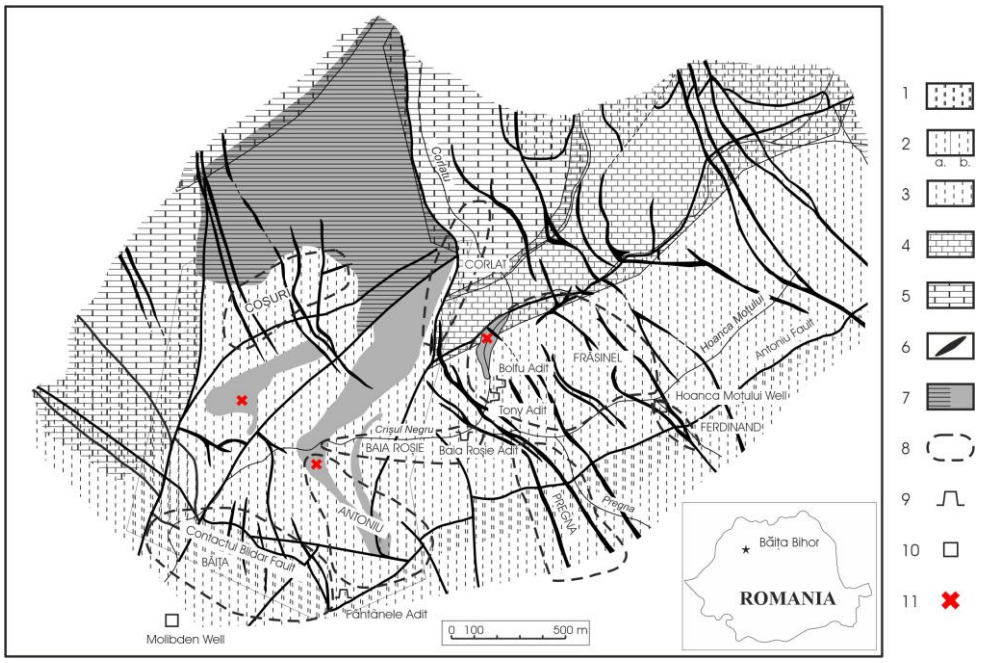

Figure 2. Geological sketch of Băiţa Bihor area (redrawn from [24] as modified by [25]). Symbols in the legend represent: 1–3—the Codru system of nappes; 1—Permian schistose clays and sandstones; 2—Triassic (Anisian–Norian) limestones (a) and dolostones (b); 3—Lower and Middle Jurassic (schistose clays, sandstones and black limestones); 4–5—the Bihor nappe; 4—Upper Jurassic (Oxfordian–Tithonic) limestones; 5—Lower Cretaceous (Barremian) limestones; 6—Upper Cretaceous—Paleogene magmatites ("banatites"): vein rocks of basaltic or andesitic composition; 7—hornfels and skarns; 8—mining field; 9—adit; 10—mining well; 11—wollastonite-bearing waste dumps. The studied sample was taken from the western waste dump.

The contact area from Băiţa Bihor, that includes about 5 square kilometers of marbles, hornfels and skarns, is located in the upper basin of the Crişul Negru River, 3.5 km ENE of Băiţa village and about 90 km south-east from the major city in the area, Oradea. The contact rocks are developed owing to the influence of an unexposed intrusive body, i.e., the Bihor batholith. The batholith consists mainly of granodiorite and granite porphyry with subordinate quartz monzodiorite and diorite: [26,27]. A whole-rock Rb-Sr isochron age of 70 ± 5 Ma has been reported for granodioritic rocks of the Bihor batholith

[28], which is in fair agreement with the K-Ar ages reported by [29], i.e., 77 ± 3 to 67 ± 3 Ma or with the U-Pb ages on zircon reported by [30], i.e., 80.3 ± 1.6 Ma. All these ages, as well as the age of mineralization (ages Re-Os of 80.63 ± 0.3 to 78.69 ± 0.4 Ma were reported by [19] on molybdenite) fit with the development of both magmatic and metallogenetic events at Băiţa Bihor during the Upper Cretaceous period.

The protolith of contact–metasomatic rocks consists of various lithologies belonging to the Bihor domain (a comprehensive sedimentary cover that lies directly upon the Bihor batholith) and Codru sedimentary nappes (a mixed sedimentary sequence overthrust on the Bihor domain at Băiţa Bihor along the Blidar Contact and Antoniu fault, shown in Figure 2). The Codru system of nappes is composed of several nappes (Batrânescu, Următ, and Vetre) that comprise a complete Triassic sequence composed of sandstones, limestones, and dolostones and is unconformably overlain by Werfenian (Lower Triassic) detrital sedimentary rocks of the Arieşeni nappe [31].

The distal skarns in the area have a carbonate protolith (limestones or dolostones) and occur as typical metasomatic columns described as "bodies" [24,26]. The wollastonite skarns are the most representative calcic skarns in the area, defining tabular bodies mainly located along the thrust zone, i.e., the Blidar Contact or Fault, which illustrates the outstanding role of the regional and local structural control: [24,26]. The most common protolith of the wollastonite skarns consists of limestones of Oxfordian–Tithonian and Barremian age that differentiate in the Bihor domain. Generally, the wollastonite skarns are monomineralic and barren; when they are mineralized, the more representative ore mineral is molybdenite, while calcic garnet can occur as associated mineral. In some metasomatic columns, the wollastonite skarn occurs in the inner zone of the column, while the outer zone is composed of diopside skarn: [26,32].

3. Material and Methods

The analyzed sample was collected from a waste dump containing silicate "gangue" of the marble quarry from Băiţa Bihor, near Băiţa Plai Mine (coordinates N 46°28′3″—E 22°37′30″). Part of the collected sample, which is quasi monomineralic, was carefully crushed, handpicked and powdered, while another split was used to produce slides and thin sections for optical, EMPA and Raman study.

A fast identification of the crystalline phases was done using X-ray powder diffraction (XRD) which was performed on two different Bruker (AXS) D8 Advance diffractometers (Bruker, Karlsruhe, Germany) hosted by the Geological Institute of Romania (Bucharest) and by the University in Liège, Belgium, respectively. Both diffractometers used Ni-filtered Cu$K\alpha$ radiation ($K\alpha_1$ = 1.54056 Å), a step size of 0.02° 2θ, and a counting time of 6 s per step. An operating voltage of 40 kV for a current of 30 mA, a slit system of 1/0.1/1 with a receiving slit of 0.6 mm, and a scanning range of 4 to 100° 2θ were used for all measurements.

XRD also served for recording more than 20 patterns of wollastonite-1*A* from galleries reaching the Blidar Fault, which are very similar to the pattern obtained for our sample. XRD quantitative phases analysis (XRD-QPA) was carried out using the Diffrac.EVA V7.3 DQUANT software (Bruker, Karlsruhe, Germany). Unit-cell parameters were calculated by least-squares refinement of the XRD data, using the computer program of Appleman and Evans [33] modified for PC use [34].

Indices of refraction were measured at room temperature (25 °C) using a conventional JENAPOL-U petrographic microscope (Carl Zeiss, Jena, Germany) with a spindle stage and calibrated immersion liquids (Cargile or temperature-calibrated oils), with a 589 nm interference filter. Thin-section photographs were obtained using a Zeiss Axio Imager A2M microscope (Carl Zeiss, Jena, Germany) with 2.5×/10×/20× objectives.

UV luminescence tests were performed using a portable Vetter ultraviolet lamp (Vetter, Lottstetten, Germany) with 254 and 366 nm filters.

Cathodoluminescence images were acquired on thin sections, using a Technosyn cold-cathode luminescence system, Model 8200 MK2 (Technosyn, Cambridge, UK), coupled to a JENAPOL-U microscope provided with a Zeiss MR C5 camera (Carl Zeiss, Jena, Germany), all of them hosted by Ecole Nationale Supérieure des Mines de Saint Etienne. The apparatus was operated at a voltage of 16 kV and a current of 400 mA.

Electron microprobe analyses (EMPAs) of silicates were performed using a CAMECA SX-50 apparatus (CAMECA, Gennevilliers, France), hosted by the Paris VI University and operating on wavelength-dispersive spectrometry. The apparatus was set at an accelerating voltage of 15 kV, a beam current of 10 nA (measured at the Faraday cup), and a beam diameter of 10 μm. Natural diopside (Si, Mg and Ca Kα), synthetic hematite (Fe Kα), natural orthoclase (K and Al Kα), natural albite (Na Kα), and natural pyrophanite (Ti and Mn Kα) served as standards. Counting time was 10 s per element. Data were reduced and corrected using the PAP procedure [35]. EMPA of the associated molybdenite was carried out using a JEOL JXA-8200 microprobe (JEOL Ltd., Tokyo, Japan), hosted by the National Research Center in Milano (Italy), operated at an accelerating voltage of 15 kV, a beam current of 15 nA, with a beam diameter of 10 μm and a counting time of 10 s per element. The standards used were galena (Pb and S Kα), forsterite (Mg and Si Kα), fayalite (Fe Kα), niccolite (As Kα) and pure metals for Mo, Cu and Zn (Kα).

Structure refinement was done by single-crystal X-ray diffraction, on a Rigaku Agilent Xcalibur EOS diffractometer equipped with a CCD detector (Rigaku Corporation, Osaka, Japan), housed at the Laboratory of Mineralogy, University of Liège. Data were collected at room temperature (293 K) with monochromatized Mo$K\alpha$ radiation (λ = 0.71703 Å) at 40 kV and 40 mA. The instrument has Kappa geometry (ϕ/ω scan). Data collection, subsequent data reduction and face-based absorption corrections were carried out using the CrysAlis Pro 41.123a software [36]. The initial solution of the structure in space group$P\bar{1}$ was determined by the charge flipping method using the Superflip algorithm [37], and the structural model was subsequently refined on the basis of F^2 with the Jana2006 software [38].

The infrared absorption spectrum of the sample chosen for study was obtained at the Geological Institute of Romania, with a SPECORD M-80 IR spectrophotometer (Carl Zeiss, Jena, Germany), using a conventional pressed-disk technique. Carefully dried mineral powders were embedded in Merk-pure KBr till a dilution of 2.5 wt.%. This spectrum was recorded between 250 and 4000 cm^{-1}. FTIR spectra of the same sample, as well as details of the stretching region of $(SiO_4)^{4-}$ groups in the wollastonite structure, were obtained using a BRUKER FTIR S 12 spectrometer (Bruker, Ettlingen, Germany) also hosted by the Geological Institute of Romania. In this case, the records were made in the frequency range between 400 and 4000 cm^{-1}, using the standard pressed-disk technique, after embedding 2 mg of mechanically ground mineral powder in 148 mg of dry KBr and compacting at 2500 N/cm^2 pressure. The spectral resolution was 0.1 cm^{-1}. All spectra were recorded at 25 °C. FTIR bands were located using the OPUS software (version 8.0) provided by Bruker.

Raman spectra were recorded on polished sections using a Renishaw SEM–Raman system (Artisan Scientific, Champaign, IL, USA) coupled with a Peltier-cooled CCD detector and hosted by the Geological Institute of Romania. Spectra were collected at 25 °C, using both structural and chemical analyze (SCA) and inVia interfaces. The spectrometer was equipped with a 50 mW, 785 nm diode-pumped solid-state laser as an excitation source. The spectral resolution was 1.5 cm^{-1} for a 1 μm spatial resolution. Analyses were collected using a 50× objective, a confocal aperture of 400 μm, a 150 μm slit width, and

1800 lines·mm^{-1} grating. The spectra were collected in the range of 113–1315 cm^{-1} (10 s accumulation time, 3 scans). Spectra were acquired using an exposure time of 10 s per frame, and 10 acquisitions at a laser power of 5%, in order to improve the signal-to-noise ratio. The instrument was calibrated with synthetic silicon, using its 520.5 cm^{-1} line. Data acquisition was carried out using Wire software version 4.4.

The mean density of various crystals of wollastonite-1*A* was measured using a pycnometer (Rainhard Co., Austin, TX, USA), at 25 °C, using a mixture of methylene iodide and toluene as the immersion liquid.

4. Results

4.1. Occurrence and Mineral Associations

At macroscopic level, wollastonite from Băița Bihor occurs as radial or sheaf-like aggregates composed of individual crystals up to 30 mm long and 1 mm wide. In many situations, these aggregates are composed of a monomineralic rock ("wollastonitite") associated only with calcite, grossular and molybdenite as ore mineral. A macroscopic view of a wollastonite—garnet sample, the same as subjected to structural refinement—is given in Figure 3, which depicts the usual scale of the crystals.

Figure 3. Hand-specimen photographs of wollastonite-bearing skarns from Băița Bihor (sample 2585). Photographs taken in natural light (**left**) and long-wave UV radiation (**right**), respectively. Diameters of the coins are 20.4 mm (**left**) and 18.2 mm (**right**) respectively.

Individual crystals are elongated along the [010] axis. The perfect cleavage on {100} can be easily observed, as well as the good cleavages on {001} and {−102}.

Molybdenite (the 2*H* polytype) is the sole ore mineral abundantly present in the wollastonite skarn. Its intensive mining during the end of the XX century could explain the abundance of wollastonite-1*A* in certain sequences of the tailing pound from Fânațe, where up to 35 vol.% wollastonite can be deduced on the basis of the XRD-QPA analysis. Molybdenite in the analyzed skarns occurs as gray-bluish pods with metallic luster in the wollastonite mass. The chemical composition of a representative sample is (in wt.% elements): Mo = 59.59, Cu = 0.12, Fe = 0.23, Mn = 0.01, and S = 40.04. The chemical structural formula corresponding to this composition, as calculated on the basis of 2 (S) per formula unit (*pfu*), is $Mo_{0.995}Cu_{0.003}Fe_{0.007}S_{2.000}$. The chemistry of molybdenite from Băița Bihor seems more complex, since [39] determined values between 0.004 and 0.013 wt.% Nb by XRF. The cell parameters of the same sample analyzed before are: a = 3.161(2) Å, b = 12.295(7) Å, and V = 106.40(5) Å^3.

Calcic garnet generally occurs as kinked bands in the wollastonite mass, suggesting infiltration metasomatism phenomena followed by tectonic movements. They are gener-

ally isotropic, with scarce optical anomalies of both sectorial and lamellar type. The index of refraction measured for a representative sample, taken as an average of ten measurements, is n = 1.745(3), corresponding to a grossular garnet.

The average chemical analysis obtained as a result of 15-point analyses performed by EMPA on three different crystals of garnet associated with wollastonite is (in wt.% oxides) SiO_2 = 39.85, TiO_2 = 0.56, Al_2O_3 = 18.29, FeO = 0.47, CaO = 35.79, MgO = 0.57, MnO = 0.14, and Na_2O = 0.01, where the partition of Fe into Fe^{2+} and Fe^{3+} was calculated using the method proposed by [40]. The chemical structural formula corresponding to this composition, calculated on the basis of five cations excepting Si *pfu* is $(Ca_{2.923}Mg_{0.064}Mn_{0.009}Fe^{2+}_{0.002}Na_{0.001})(Al_{1.628}Fe^{3+}_{0.335})(Si_{2.962}Ti_{0.032}Al_{0.006})O_{11.940}$. The formula corresponds to a grossular garnet (Grs 82.88 mol.%, Adr 17.12 mol.%). As O < 12 *apfu*, a hydrogarnet component could be suspected.

4.2. Physical Properties and Crystal Chemistry

The macroscopic color is typically snow white. The mineral is slightly luminescent under long-wave (366 nm) ultraviolet radiation, the luminescence tint being light blue (Figure 3). The powders show a strong cathodoluminescence in blue tints, which is also evident on some thin sections and associates with the bright green cathodoluminescence color reported previously (e.g., [41]): Figure 4.

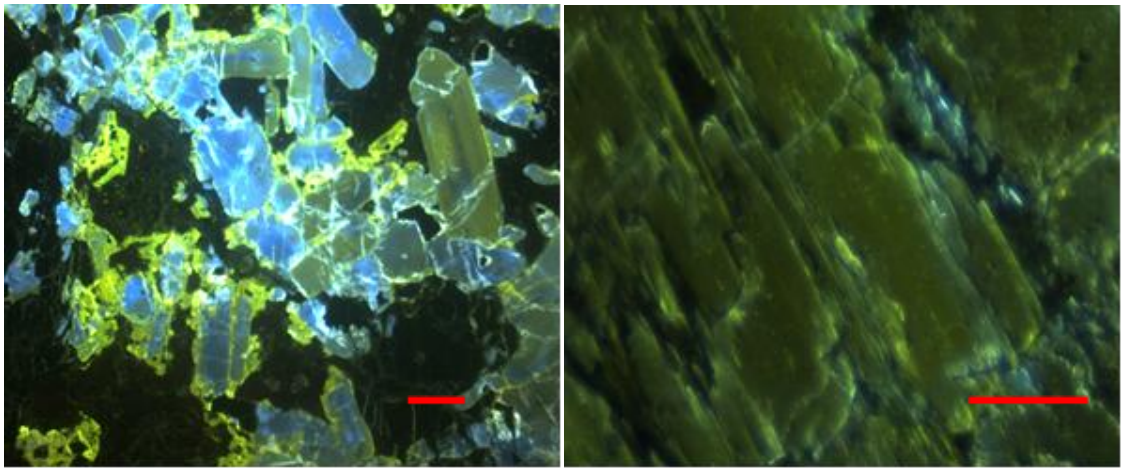

Figure 4. Cathodoluminescence images of wollastonite-1*A* from Băița Bihor. The scale bars represent 1 mm.

As expected, wollastonite from Băița Bihor is biaxial negative, with an optical angle of $2V_\alpha$ = 39°. The measured refractive indices are α = 1.616, β (calc.) = 1.629 and γ = 1.631. The mean index of refraction is $\overline{n}$ = 1.625. The crystals display parallel extinction. The birefringence colors are located at the end of the first order of the Michel-Levy chart (Figure 5).

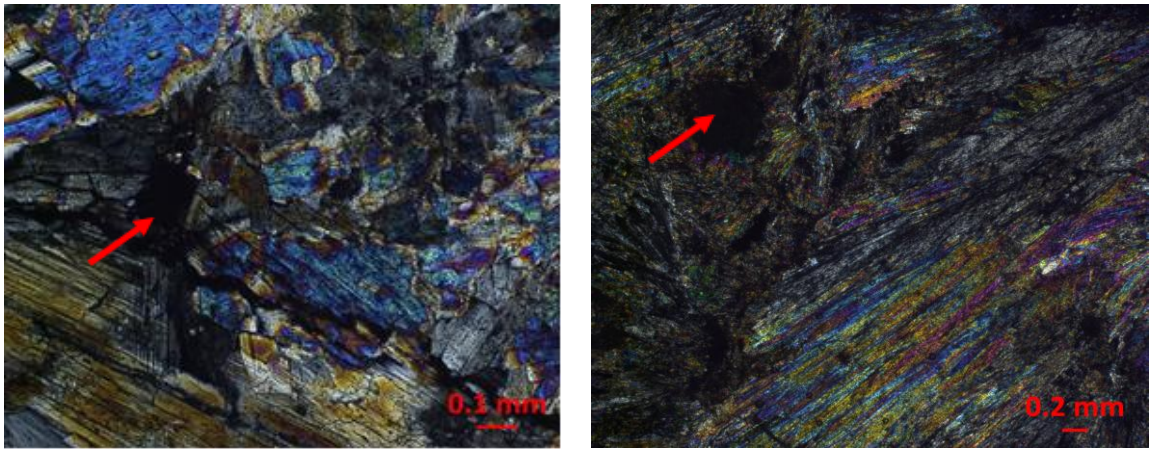

Figure 5. Photomicrographs showing characteristic relationships between wollastonite-1*A* and associated minerals. Crossed polars. The arrows indicate inclusions of molybdenite (**left**) and grossular (**right**) in the wollastonite-1*A* mass.

The chemical (EMPA) analysis of ten different crystals of wollastonite from a representative sample, as well as the formulas normalized on the basis of three oxygen atoms per formula unit (*apfu*), is given as Supplementary Material (Table S1). No chemical zoning or inhomogeneity was observed across the same crystal. As can be observed, the analyses exhibit only relatively small deviations from the ideal composition. The average composition deduced from the data in Table S1 is (in wt.% oxides) SiO_2 = 51.68, TiO_2 = 0.07, Al_2O_3 = 0.18, FeO = 0.04, MnO = 0.04, MgO = 0.06, CaO = 48.57, which yields the chemical structural formula $(Ca_{1.000}Mg_{0.002}Mn_{0.001}Fe_{0.001})(Al_{0.004}Ti_{0.001}Si_{0.994})O_3$, which closely approximates the ideal $CaSiO_3$. The wet chemical analysis reported by Loczka [10], i.e., (in wt.% oxides): SiO_2 = 51.61, CaO = 46.20, FeO = 0.51, MnO = 0.47, MgO = 1.08, K_2O = 0.13, Na_2O = 0.11, H_2O = 0.54, clearly corresponds to an impure sample, which most probably contains diopside and talc.

The mean measured density, taken as an average of measurements on 10 different grains, is D_m = 2.922(3) g/cm^3, which compares well with the calculated density, obtained on the basis of the molecular mass derived from the chemical data given before (i.e., M = 116.261 g/mol) and of the unit-cell volume determined by structure refinement (see below) for Z = 6 formula units per cell (e.g., Refs. [42,43]), i.e., D_x = 2.916 g/cm^3.

As derived from the mean refractive index given before and from the measured density, the physical refractive energy is K_p = 0.2139. The chemical refractive energy (K_C) value, based on the formula given before and on the constants of [44], is K_c = 0.2091. The calculation of the Gladstone–Dale compatibility index ($1 - K_p/K_c$) yielded a value of −0.023, indicative of an excellent agreement between physical and chemical data [44]. The physical refractive energy calculated on the basis of the calculated value of density is K_p = 0.2143. The use of this value in the calculation does not substantially influence the compatibility index which is −0.025 and remains "excellent" as ranked by [44].

4.3. Structure

The structure of wollastonite-1*A* was successfully refined using two-dimensional film data [43], and confirmed as reliable [45–49]. More accurate refinements by [50–55] described practically the same structure.

The structure consists of infinitely long single chains of SiO_4 tetrahedra, two of them having a common O corner and being paired to a third silicon tetrahedron [55]. In all wollastonite polytypes, the chains of tetrahedra, running along the *b* axis, are characterized by

a periodicity of three. The chains are held together by interstitial Ca which is in a distorted six-fold coordination. In other words, the structure may be regarded as built up of SiO_3 chains and Ca_3O_3 laths, both running parallel to the *b* axis and sharing oxygen atoms among them [56]. "Partial mirrors" or reflection planes that appear in the crystal structure and do not respect the standard extinction conditions for the structural group were identified by some authors based on XRD study [57]. These "partial mirrors", which are discontinuous within the structure, signify that the wollastonite structure can accommodate variations in stacking, which define polytypes.

A Rietveld structure refinement of wollastonite crystals from Băiţa Bihor reported previously [14] was based on very few reflections from the X-ray powder pattern. In the limit of errors, the wollastonite refined by these authors could be triclinic, with the occurrence of the 1*A* polytype being the most probable. The structural refinement of a representative sample of wollastonite-1*A* from Băiţa Bihor (Sample 2585) was consequently done both in order to supplement the data on the mineral structure and to identify the real polytype present in the skarns from Băiţa Bihor. Table 1 depicts the data collection and structure refinement details for the analyzed sample. The original *.cif file obtained during the structural refinement of the analyzed sample can be obtained under request from the first author.

Table 1. Details of the X-ray data collection and refinements of wollastonite-1*A* from Băiţa Bihor.

Crystal Data	
Crystal shape	acicular
Color	white
Crystal size (mm)	0.11 × 0.15 × 0.30
Temperature (K)	293(2)
a (Å)	7.9233(3)
b (Å)	7.3203(3)
c (Å)	7.0651(3)
α (°)	90.053(3)
β (°)	95.208(3)
γ (°)	103.384(3)
V (Å^3)	396.91(3)
Crystal system	triclinic
Space group	$P\bar{1}$
Z	6
Formula weight	116.17
$D_{calc.}$ (g/cm^3)	2.916
Data collection	
Diffractometer	Rigaku Xcalibur, CCD detector
Radiation; λ	MoK_α; 0.71073
Absorption coefficient (mm^{-1})	2.566
F(000)	348
2ϴ range for data collection (°)	5.3 to 57.72°
Range of indices	$-10 \le h \le 10$ $-9 \le k \le 9$ $-9 \le l \le 9$
Number of measured reflections	8757
Number of unique reflections	1928
Criterion for observed reflections	$I > 2\sigma(I)$
Refinement	
Refinement on	Full-matrix least squares on F^2
Data/restraints/parameters	1928/0/136

https://doi.org/10.3390/cryst16040247

R_1 (F) with $F_0 > 2\sigma(F_0)$ *	$R_1 = 0.0678$, $wR_2 * = 0.1688$
R_1 (F) for all the unique reflections *	$R_1 = 0.0776$, $wR_2 * = 0.1846$
S ("goodness of fit")	1.067
Weighing scheme	$1/(\sigma^2(I)^2 + 0.0049(I)^2$
Min./max. residual e density, (eÅ^{-3})	−0.952/5.043

* $R_1 = \Sigma(|F\text{obs}| - |F\text{calc}|)/\Sigma|F\text{obs}|$; $wR_2 = \{\Sigma[w(F^2\text{obs} - F^2\text{calc})^2]/\Sigma[w(F^2\text{obs})^2]\}^{1/2}$. $W = 1/[s^2(F_0^2) + (aP)^2 + bP]$, where $P = [2F_c^2 + \text{Max}(F_0^2, 0)]/3$, where a, b are shown in the refinement process.

The cell parameters in Table 1 are similar to the data given by [45], i.e., a = 7.94 Å, b = 7.32 Å, c = 7.07 Å, α = 90.02°, β = 95.22°, and γ = 103.26°, or to the more accurate data refined by [51], i.e., a = 7.9258(4) Å, b = 7.3202(4) Å, c = 7.0653(4) Å, α = 90.055(3)°, β = 95.055(3)°, and γ = 103.426(3)°; [54], i.e., a = 7.9285(4) Å, b = 7.3234(3) Å, c = 7.0684(4) Å, α = 90.077(4)°, β = 95.201(5)°, and γ = 103.399(4)°; or [55], i.e., a = 7.0786(16) Å, b = 7.3309(4) Å, c = 7.079(2) Å, α = 90.07(2)°, β = 95.30(2)°, and γ = 103.41(2)° (re-oriented for $a > b > c$).

For a better view of the structure, Table 2 gives the fractional atomic coordinates (×10^4) whereas Table 3 offers the equivalent isotropic displacement parameters (Å^2 × 10^3) for wollastonite-1*A* from Băița Bihor. The refined structure is shown in Figure 6.

Table 2. Fractional atomic coordinates (×10^4) and equivalent isotropic displacement parameters. (Å^2 × 10^3) for wollastonite-1*A* from Băița Bihor.

Atom	x	y	z	U_{eq} *
Ca1	2976.0(13)	714.3(13)	2362.1(13)	8.0(3)
Ca2	3011.9(13)	−4227.7(12)	2390.2(13)	7.7(3)
Ca3	32.5(12)	−2496.4(12)	5246.8(14)	9.5(3)
Si1	6845.0(18)	−476.0(19)	2694.2(18)	9.5(3)
Si2	1029.3(18)	2762.4(18)	−558.1(19)	10.5(4)
O1	4812(5)	−1327(5)	2646(5)	10.7(7)
O2	973(5)	2729(5)	1723(5)	10.3(7)
O3	4827(5)	3736(5)	2646(5)	10.7(7)
O4	723(5)	−2305(5)	1976(5)	10.1(7)
Si3	6851.0(18)	3896.3(19)	2686.1(18)	9.5(3)
O5	8019(5)	−592(5)	4648(5)	9.5(7)
O6	8037(5)	4602(5)	4642(5)	8.5(7)
O7	7717(5)	−1289(5)	939(5)	14.7(8)
O8	2265(5)	4873(5)	−924(5)	14.8(8)
O9	7182(5)	1789(5)	2249(5)	17.1(8)

* U_{eq} is defined as 1/3 of the trace of the orthogonalized U_{IJ} tensor.

Table 3. Anisotropic displacement parameters (Å^2 × 10^3) for wollastonite-1*A* from Băița Bihor *.

Atom	U_{11}	U_{22}	U_{33}	U_{23}	U_{13}	U_{12}
Ca1	10.5(5)	5.7(5)	8.5(5)	0.8(3)	1.6(4)	2.8(4)
Ca2	9.5(5)	3.9(5)	8.9(5)	−0.9(3)	1.3(4)	0.1(4)
Ca3	9.0(6)	4.3(5)	15.1(5)	0.4(3)	2.1(4)	1.2(4)
Si1	7.7(7)	12.2(7)	7.8(6)	−0.9(5)	0.7(5)	0.6(5)
Si2	12.0(7)	7.8(6)	11.3(7)	−0.8(5)	0.8(5)	2.0(5)
O1	7.8(17)	6.1(16)	17.4(18)	−1.3(13)	0.3(14)	0.7(13)
O2	11.4(18)	6.6(15)	12.7(17)	−1.1(12)	−2.1(13)	2.9(13)
O3	6.2(17)	8.5(16)	16.6(18)	0.4(13)	0.1(13)	0.4(13)
O4	13.2(18)	7.3(16)	9.5(16)	−0.6(12)	−1.4(13)	2.4(13)
Si3	7.8(7)	12.3(7)	7.8(6)	−0.6(5)	0.3(5)	0.9(5)
O5	12.1(18)	9.6(16)	7.8(16)	0.0(12)	0.8(13)	4.9(14)
O6	9.9(17)	7.6(15)	6.9(15)	−0.4(12)	−0.4(12)	−0.2(13)
O7	19(2)	11.2(17)	14.4(18)	−3.2(13)	−0.3(14)	6.0(15)
O8	20(2)	9.1(17)	14.2(18)	0.1(13)	1.5(14)	0.5(14)
O9	21(2)	9.3(17)	21.2(19)	−0.4(14)	4.9(15)	3.6(15)

* The anisotropic displacement factor exponent is calculated as $-2\pi^2[h^2a^{*2}U_{11} + \ldots + 2hka \times b \times U_{12}]$.

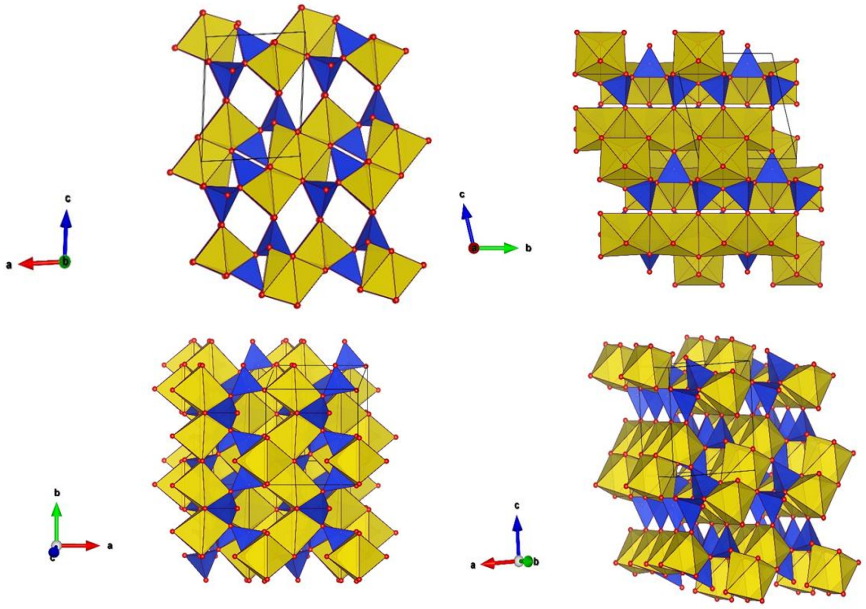

Figure 6. Projections of the structure of wollastonite-1*A* from Băița Bihor along various axes, showing the coordination polyhedra. The dark blue tetrahedra represent SiO_4, the gray–yellow polyhedra represent CaO_6 octahedra and the red balls represent O^{2-} corners. **Top**: Projection of the structure on (010), showing the unit cell and the three tetrahedral chains (**left**), and at the level of formula unit (**right**). **Bottom**: Projection of the structure on (001) showing the stacking along the *a* axis—**left**; and projection on (010), showing the assemblage of structural columns and laths specific to pyroxenoids (**right**).

The crystal structure consists of single chains of edge-sharing SiO_4 tetrahedrons running along the *b* axis, with a strong tendency to form Si_3O_9 groups from corrugated tetrahedra along the *c* axis. The chains are linked by three columns of distorted CaO_6 octahedra, with Ca-O bond lengths of 2.264–2.652 Å as it can be seen in Table 4 in the text and S3 from the Supplementary Materials.

Table 4. Selected bond lengths for wollastonite-1*A* from Băița Bihor.

Atom	Atom	Length (Å)	Atom	Atom	Length (Å)
Ca1	O1	2.311(4)	Si1	O1	1.584(4)
Ca1	O2	2.419(4)	Si1	O5	1.607(4)
Ca1	O3	2.351(4)	Si1	O7	1.647(4)
Ca1	O4	2.496(4)	Si1	O9	1.653(4)
Ca1	O5 ^{3}	2.316(4)	Mean		1.623(4)
Ca1	O7 ^{2}	2.408(4)			
Mean		2.384(4)	Si2	O2	1.616(4)
			Si2	O4 ^{6}	1.605(4)
Ca2	O1	2.264(3)	Si2	O7 ^{2}	1.663(4)
Ca2	O2 ^{5}	2.447(4)	Si2	O8	1.661(4)
Ca2	O3 ^{5}	2.296(4)	Mean		1.636(4)
Ca2	O4	2.539(4)			
Ca2	O6 ^{3}	2.318(4)	Si3	O6	1.612(4)
Ca2	O8 ^{5}	2.415(4)	Si3	O8 ^{12}	1.649(4)
Mean		2.380(4)	Si3	O9	1.657(4)
			Mean		1.639(4)
Ca3	O2 ^{1}	2.344(4)			

Ca3	O4	2.419(4)
Ca3	O5 [7]	2.361(4)
Ca3	O5 [3]	2.421(4)
Ca3	O6 [8]	2.348(3)
Ca3	O6 [3]	2.406(4)
Mean		2.383(4)

[1] −X, −Y, 1 − Z; [2] 1 − X, −Y, −Z; [3] 1 − X, −Y, 1 − Z; [5] +X, −1 + Y, +Z; [6] −X, −Y, −Z; [7] −1 + X, +Y, +Z; [8] −1 + X, −1 + Y, +Z; [12] 1 − X, 1 − Y, −Z.

The linkage of tetrahedra and octahedra at the apical oxygens of the tetrahedra is better depicted in Figure 6. It can be seen that in the crystal structure, one O-O edge of octahedra is connected to adjacent SiO_4 tetrahedra to form a Si_2O_7 group and another across a third tetrahedron [50]. As a result, the octahedral sites involve both bridging and non-bridging oxygens, with the bridging oxygens sites tending to show relatively large changes as compared with the non-bridging ones, which directly influence the vibrational behavior (see below). The Si-O and Ca-O distances in Table 4, transposed in Figure 6, illustrate the mismatch between the tetrahedral repeat units and the octahedral bands [53]. Consequently, the tetrahedra are tilted to accommodate their apices to the octahedral ones, as already observed by [45,48,50–53,55]. As a consequence, the SiO_4 tetrahedra are in turn deformed, with Si-O distances varying between 1.578 and 1.663 Å (Table 4). As in all the other pyroxenoids, the inversion-related tetrahedra chains are organized in pairs that run along the *b* axis, which represent one basic slab of the structure (e.g., [53,55]). The tetrahedra chains are shifted relative to each other, changing the periodical basis along the *a* axis. The stacking characteristic to the 1*A* polytype, which contains a sole slab along the *a* axis [53–55], can be observed in Figure 6.

The collection of angles in Table S4, as well as the torsion angles given in Table S2 (Supplementary Materials), reflects a much-distorted structure, characteristic of the 1*A* polytype.

4.4. Infrared and Raman Behavior

The IR, FTIR and Raman spectra recorded for representative wollastonite-1*A* samples from Băița Bihor are given in Figures 7 and 8, respectively, while Table 5 offers an attempt to assume the vibrational bands in the Raman and infrared spectra to specific vibrational modes, together with the character and relative intensities of the bands in the infrared spectra.

Table 5. Positions and assignments of the IR and Raman bands recorded for a selected sample of wollastonite-1*A* from Băița Bihor [(1)].

Structural Group	Vibrational Mode	Wavenumber (cm^{-1})			Character, Intensity [(2)]
		IR	Raman	FTIR	
SiO_4	ν_3 O_b-Si-O_b antisymmetric stretching	1084	1043	1089	sh, s
SiO_4	ν_3 Si-O_b-Si antisymmetric stretching	1026	1020	1060	sh, s
SiO_4	ν_3' Si-O_b-Si antisymmetric stretching	1004	997	1019	sh, vs
SiO_4	ν_1 O_n-Si-O_n symmetric stretching	960	970	966	sh, s
SiO_4	ν_3 O_b-Si-O_n antisymmetric stretching	940	-	929	sh, vs
SiO_4	ν_3' O_b-Si-O_n antisymmetric stretching	908	-	903	sh, vs
SiO_4, CaO_6	Ca–O–Si vibration	876	889	-	sh, s
SiO_4	ν_1 Si-O_n-Si symmetric stretching	692	688	682	sh, w
SiO_4	ν_1' Si-O_n-Si symmetric stretching	652	635	644	sh, m
SiO_4	ν_2 O-Si-O out-of-plane bending	581	577	582	shd, m
SiO_4	ν_2 Si-O_n-Si out-of-plane bending	562	-	567	sh, m

SiO4	ν_2' Si-O_n-Si out-of-plane bending	518	-	-	sh, m
SiO_4	ν_2'' Si-O_n-Si out-of-plane bending	500	507	509	sh, s
SiO_4	ν_2 Si-O_b-Si out-of-plane bending	472	466	471	sh, vs
SiO_4	ν_2' Si-O_b-Si out-of-plane bending	462		453	sh, vs
		445	-	-	shd, m
		412	412	407	sh, w
		345	335	-	sh, m
		320	323	-	sh, m
CaO_6	lattice vibrations (?)	302	-	-	shd, w
		280	-	-	sh, w
		265	235	-	sh, w
		-	168	-	-

(1) Assumptions according to the authors referred in text; (2) character of the bands on IR spectra: s = strong; m = medium; w = weak; vs = very strong; sh = sharp; shd = shoulder.

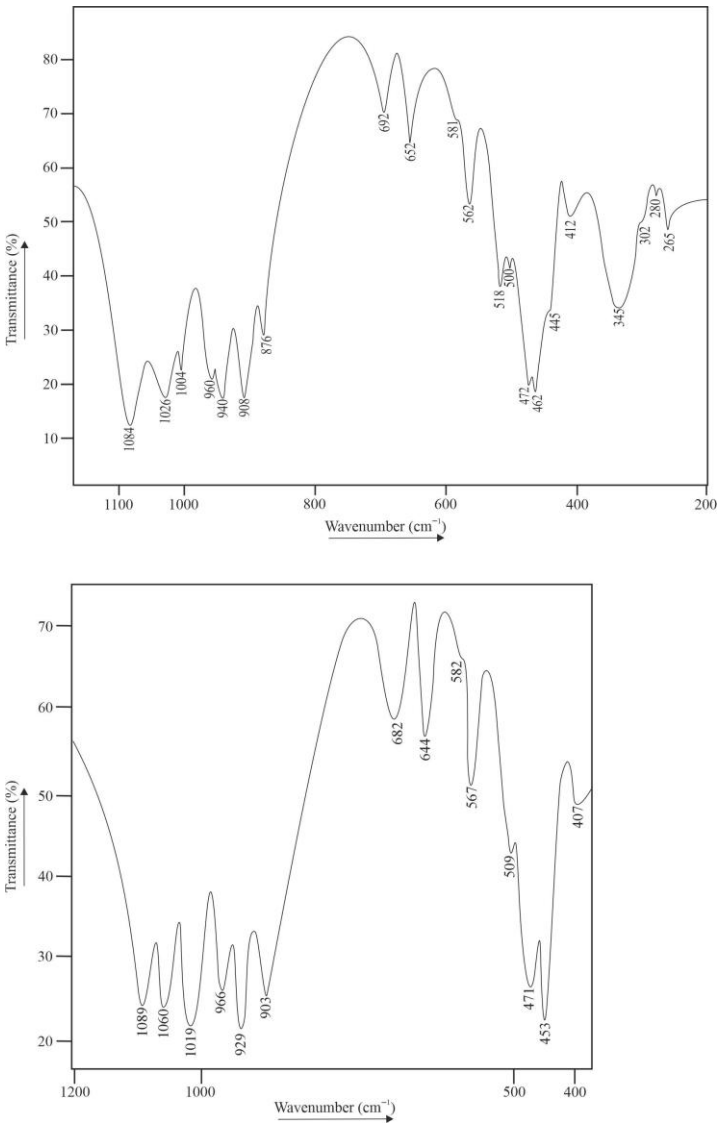

Figure 7. Infrared (**top**) and Fourier transform infrared (**bottom**) spectra of a selected sample of wollastonite-1*A* from Băiţa Bihor (Sample 2585).

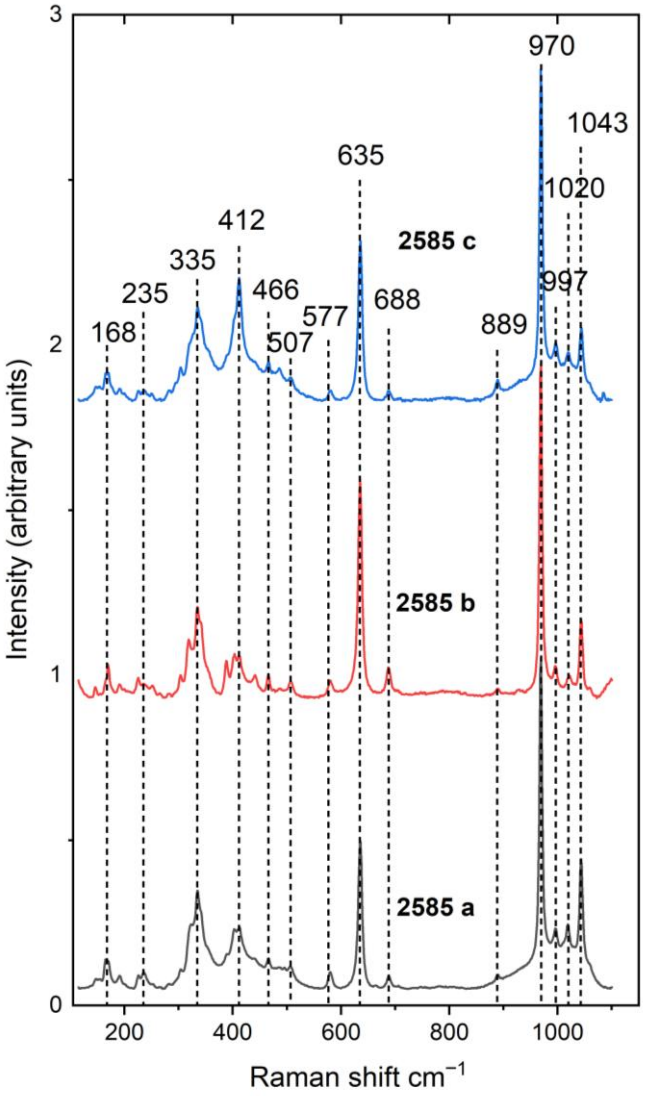

Figure 8. Raman spectra recorded for different crystals of wollastonite-1*A* from Băița Bihor (Sample 2585).

At first look, the IR and Raman spectra of wollastonite-1*A* are identical with similar spectra recorded for the more ordered 2*M* polytype, but the bands in the IR spectra seem broader. In fact, the lower crystallinity of the 1*A* as compared with that of the 2*M* polytype conduces to a more advanced amorphization during milling [58] and grinding [59] and could explain the broader absorption bands in the spectra of triclinic wollastonite, observed in some of the recorded spectra.

The assumption of the bands in the spectra in Figures 7 and 8 and Table 5 is considerably facilitated by studies on $CaSiO_3$ slags and glasses [60–62] and by the studies of [59,63–65] for infrared, and of [66,67] for the Raman behavior of wollastonite.

The main bands in the IR and Raman spectra can be assumed, as expected, to Si-O and Ca-O vibrations. From higher to lower wavenumbers, three groups of bands, involving Si-O vibrations, can be distinguished, as follows:

(1) A group of three intense bands materializing the Si-O-Si antisymmetric stretching of bridged oxygens, in the frequency range 1018–1087 cm^{-1}; on Raman spectra, this antisymmetric stretching seems only double degenerate (Table 5). Note that bands at ~ 990 and 1090 cm^{-1} were found in chain- and sheet-structured species containing Ca and SiO_4 tetrahedra, respectively, which fits with our structural data [61].

(2) Another group of three bands, occurring at ~ 960, 940 and 908 cm^{-1}, materialize Si-O-Si stretching vibrations involving non-bridged oxygens. Only two corresponding bands are retrieved on the Raman spectra and are considered characteristic of SiO_4 tetrahedra linked laterally by Ca ions [68] as they were observed in both wollastonite and diopside.

(3) The symmetric Si-O-Si stretching is, on its turn, materialized by another triplet of bands recorded on the IR spectrum, at 652, 660 and 692 cm^{-1}. These bands were assigned by [60] and [62] to Si-O-Si bending vibrations within SiO_4 tetrahedron, but this kind of vibrations must occur at lower frequencies. In the Raman spectra, the Si-O-Si symmetric stretching also seems to be double degenerate, being materialized by the bands at 636 and 688 cm^{-1}, located at the same wavenumbers found by [66].

Apart from these triplets, a vibration band located in the IR spectra at 876 cm^{-1}, which is also Raman-active (band at 889 cm^{-1}), can be ascribed to Ca-O-Si vibrations [62].

The corresponding out-of-plane Si-O-Si bending modes occur in the infrared spectra, in the 500–570 cm^{-1} region at ~500, 518 and 562 cm^{-1}, being completed by an in-plane bending at 472 cm^{-1}. The Raman bands corresponding to Si-O-Si bending vibrations are recorded at 507 and 577 cm^{-1}, respectively.

The IR absorption bands at lower wavenumbers in the infrared spectrum (i.e., 462, 445, 412, 345, 320, 302, 280, and 265 cm^{-1}) could be ascribed to the stretching vibrations of the calcium–oxygen bond and are generally doubled by equivalent Raman bands.

All the bands that can be assigned to vibrations involving SiO_4 tetrahedra in the IR spectrum are triple degenerate, reflecting the number of three tetrahedra in the chain repeat unit.

Note that bands assignable to CO_3 groups and particularly to the antisymmetric O-C-O stretching vibrations at ~1430 and 1385 cm^{-1} were observed in the IR and FTIR spectra. They could be due to both the admixed calcite, but also as an effect of wollastonite carbonation due to the grinding [59].

5. Discussion

As in most occurrences of wollastonite described in the literature (e.g., [2,55] and references therein), wollastonite from Băița Bihor occurred as a product of the reaction of calcite and quartz (in wollastonite-bearing marbles) or by silica metasomatism of calcite from limestones and dolostones (in skarns), through the reaction

$SiO_2 + CaCO_3 = CaSiO_3 + CO_2$ (e.g., [53,69–71] and referred works).

As observed by [72], the formation of high-grade, commonly mono- or bimineralic skarn deposits could be more convincingly ascribed to infiltration metasomatism [73], in which invading fluids generate specific reactions until an original mineral (in our case calcite or dolomite) or mineral assemblage (calcite + dolomite) is destroyed. This is clearly the case at Băița Bihor, where the formation of skarns is ascribed to the interaction between magmatically derived silica-rich and CO_2-poor fluids emerging from the magmatic body and marbles, rather than to thermal metamorphism and metasomatism of silica-rich marbles, which were not identified in the area.

We estimate that the mineral crystallized at temperatures of around 550–600 °C, at pressures up to 3 kbar [25]. These temperatures, in agreement with those estimated for the crystallization of wollastonite at low pressures [69], are much lower than those obtained during the cooling of $CaSiO_3$ glass (i.e., 900–950 °C: [53]), due to both the longer duration of the thermal influence at the contact and to the higher fluid pressure. The crystallization at lower temperatures, up to 500 °C [3,74], is not sustained by the textural relations with the paragenetic grossular. Textural and chemical particularities indicate that the mineral formed as a member of the peak thermal–metasomatic assemblage, together with grossular and diopside. Structural evidence shows any transition toward the

1*Td* completely disordered the metastable polytype, which could signify the evolution toward the higher-temperature polytype, wollastonite-2*M* (e.g., [53]).

A high-temperature hydrothermal stage of evolution of the wollastonite-1*A* skarn failed to alter wollastonite into zeolites or CSH minerals (e.g., plombièrite, tobermorite, xonotlite) as in the high-temperature skarns. Molybdenite-2*H* is the main ore mineral crystallized in this stage and does not show a brutal decrease in temperature, compatible with the crystallization of CSH phases. In fact, this higher-temperature polytype of molybdenite crystallizes at much higher than 500 °C (e.g., [39] and references inside). The contents of niobium mentioned in the Băița Bihor molybdenite [39] are consistent with the high temperatures of crystallization, in accord with the experiments of [75]. In this case, it is easy to consider that the first phase of hydrothermal evolution of the skarn system involved conditions of equilibrium between wollastonite skarn and early hydrothermal fluids. No signs of later hydrothermal phases were found in the studied skarn.

6. Conclusions

Our study fully confirms that the lower-temperature polytype of β-$CaSiO_3$ present in the contact area from Băița Bihor is wollastonite-1*A*, in good agreement with previous observations [2], experiments [53] and phase diagrams [55,71]. The structure refinement reported by [14], which identified the higher-temperature 2*M* polytype at Băița Bihor, appears to be incorrect.

Physical and crystallographic properties, vibrational behavior, as well as crystal chemistry show that wollastonite-1*A* from Băița Bihor is very close to stoichiometry. In this case, the assumption of [50] that the admission in the octahedral sites, normally occupied by Ca, of other cations, with smaller ionic radii (e.g., Mg, Fe, Mn), distorting the structure and favoring the crystallization of the 1*A* polytype, is not fully sustained.

As expected, the infrared and Raman behavior of wollastonite-1*A* does not essentially differ from those of other polytypes [65,66], showing that the differences in stacking do not essentially influence the vibrations characteristic to structural groups.

Supplementary Materials: The following supporting information can be downloaded at: https://www.mdpi.com/article/10.3390/cryst16040247/s1, Table S1. EMPAs of a representative sample of wollastonite-1*A* from Băița Bihor. Table S2. Torsion angles for a selected sample of Wollastonite-1*A* from Băița Bihor. Table S3. Bond lengths for wollastonite-1*A* from Băița Bihor. Table S4. Bond angles for wollastonite-1*A* from Băița Bihor.

Author Contributions: Conceptualization, Ş.M., D.-G.D., C.S.G., F.H. and M.D.; formal analysis, Ş.M., C.S.G., D.-G.D., M.D., F.H. and A.-M.I.; funding acquisition, Ş.M., D.-G.D., C.S.G. and F.H.; investigation, Ş.M., D.-G.D., F.H., C.S.G., M.D., G.D. and A.-M.I.; methodology, Ş.M., D.-G.D. and F.H.; resources, Ş.M., D.-G.D., F.H. and C.S.G.; data curation, Ş.M., D.-G.D., C.S.G., F.H. and M.D.; writing—original draft preparation, Ş.M.; writing—review and editing, Ş.M.; visualization, Ş.M.; supervision, Ş.M.; project administration, Ş.M., D.-G.D., C.S.G. and F.H. All authors have read and agreed to the published version of the manuscript.

Funding: This study was partly supported by a scientific cooperative research grant awarded by the Walloon and Romanian Governments (1 BMBE/2024). Other grants allowed to the first author by UEFISCDI in Romania (PN-III-P1-1.2-PCCDI-2017-0346 and PN-III-P1-1.1-MC-2018-3163) and by the Ministry of Education and Research (PN23-39-02-01/2023, PN23-39-02-06/2023 and PN23-39-02-07/2023) generously supported the final draft. C.S. and A.-M.I. gratefully acknowledge receipt of two UEFISCDI grants (PN-III-P1-1.1-MC-2018-3199 and PN-III-P1-1.1-MC-2018-3211) which helped to obtain part of the structural, DRX and FTIR data.

Data Availability Statement: Most of the data that substantiated this study are available on request from the first author. Data for structure refinements, including *.cif files, are available on request from the third author (fhatert@uliege.be).

Acknowledgments: The assistance of Michel Fialin (Université Paris VI) in the electron microprobe work, and of Gabriela Stelea (Geological Institute of Romania, Bucharest) in the IR acquisition is gratefully acknowledged. Fabrice Dal Bo, Corentin Amador del Valle (University in Liège) and Pietro Vignola (Italian National Research Council—University in Milan) kindly communicated some of the XRD and EMPA data used for this study. Fruitful discussions on the field with the late Jean Verkaeren, with André-Mathieu Fransolet, Bernard Guy, Essaïd Bilal, Gheorghe Ilinca, Jacqueline Vander Auwera, Marie Lola Pascal, Hans-Peter Schertl, Walter Maresh, Evgheny Galuskin, Irina Galuskina, Robert Martin and Maxime Baijot are highly appreciated. Members of staff of SC Băiţa Bihor SA and Vast Resources PLC—Băiţa Plai mining companies are gratefully acknowledged for their assistance in the field and sampling activities.

Conflicts of Interest: The authors declare no conflicts of interest. The funders had no role in the design of the study; in the collection, analyses, or interpretation of data; in the writing of the manuscript; or in the decision to publish the results.

References

1. Fleischer, M.; Mandarino, J.A. *Glossary of Mineral Species*, 7th ed.; The Mineralogical Record Inc.: Tucson, AZ, USA, 1995; pp. 1–280.
2. Deer, W.A.; Howie, R.A.; Zussman, J. *An Introduction to the Rock-Forming Minerals*, 2nd ed.; Longman: Harlow, UK, 1992; pp. 1–696.
3. Virta, R.L.; Van Gosen, B.S. Industrial Minerals of the United States. In *Wollastonite—A Versatile Industrial Mineral*; USGS Fact Sheet FS-002-01; USGS Publications Warehouse: Reston, VA, USA, 2001.
4. Andrews, R.W. *Wollastonite*; Her Majesty's Stationery Office: London, UK, 1970; pp. 1–114.
5. Spencer, C.H. *Mémento Roches et Minéraux Industriels—Wollastonite*; BRGM: Orléans, France, 1991; pp. 1–32.
6. Bauer, R.R.; Copeland, J.R.; Santini, K. Wollastonite. In *Industrial Minerals and Rocks*, 6th ed.; Carr, D.D., Ed.; Society for Mining, Metallurgy, and Exploration, Inc.: Littleton, CO, USA, 1994; pp. 1119–1128.
7. Azarov, G.M.; Maiorova, E.V.; Oborina, M.A.; Belyakov, A.V. Wollastonite raw materials and their applications (a review). *Steklo i Keramika* **1995**, *9*, 13–16. (In Russian)
8. U.S.G.S. *Mineral Commodity Summaries—Wollastonite*; US Geological Survey: Reston, VA, USA, 2023; pp. 194–195.
9. von Zepharovich, V.R. *Mineralogisches Lexicon des Kaisertums Österreich*; Volume 2; Braumüller, W., Ed.; Wien: 1873; pp. 1–451, https://www.lehmanns.de/shop/naturwissenschaften/52340706-9783750197633-mineralogisches-lexikon-fuer-das-kaisertum-oesterreich
10. Loczka, J. Mineral-Chemische Untersuchungen. *Z. Kristallogr. Miner.* **1885**, *10*, 89–90.
11. Udubaşa, G.; Ilinca, G.; Marincea, Ş.; Săbău, G.; Rădan, S. Minerals in Romania: The state-of-the-art 1991. *Rom. J. Miner.* **1992**, *75*, 1–51.
12. Andrii, M.P.; Tămaş, G.C. Ore mineralogy and geochemistry relationships in Băiţa Bihor ore deposit, Apuseni Mountains, Romania—Blidar Contact case study. *Rom. J. Miner. Dep.* **2018**, *91*, 49–53.
13. Tămaş, C.G.; Andrii, M.-P. Mineralogy of skarn ores from Băiţa Bihor, Northern Apuseni Mountains, Romania: A case study of Cu-, Bi- and Sn-minerals. *Minerals* **2020**, *10*, 436.
14. Brănoiu, G.A.; Cristescu, T. The Rietveld structure refinement of the wollastonite-2*M* crystals from Băiţa Bihor deposit (Romania) using X-ray powder diffraction data. In *Science and Technologies in Geology, Exploration and Mining. Conference Proceedings, Vol. 1, 13th International Multidisciplinary Scientific Geoconference SGEM, Albena, Bulgaria, 15–21 June 2013*; Sofia STEF92 Technology 2013, pp. 217–223.
15. Berza, T.; Constantinescu, E.; Vlad, Ş.N. Upper Cretaceous magmatic series and associated mineralization in the Carpatho-Balkan Orogen. *Res. Geol.* **1998**, *48*, 291–306.
16. Gallhofer, D.; von Quadt, A.; Peytcheva, I.; Schmid, S.M.; Heinrich, C.A. Tectonic, magmatic, and metallogenic evolution of the Late Cretaceous arc in the Carpathian-Balkan orogen. *Tectonics* **2015**, *34*, 1813–1836.

17. Cioflică, G.; Vlad, Ş. The correlation of the Laramian metallogenetic events belonging to the Carpatho-Balkan area. *Rev. Roum. Géol. Géophys. Géogr. Sér. Géol.* **1973**, *17*, 217–224.
18. Ciobanu, C.L.; Cook, N.J.; Stein, H. Regional setting and geochronology of the Late Cretaceous Banatitic Magmatic and Metallogenetic Belt. *Miner. Depos.* **2002**, *37*, 541–567.
19. Zimmermann, A.; Stein, H.; Hannah, J.; Koželj, D.; Bogdanov, K.; Berza, T. Tectonic configuration of the Apuseni-Banat-Timok-Srednogorie belt, Balkans-Southern Carpathians, constrained by high precision Re-Os molybdenite ages. *Miner. Depos.* **2008**, *43*, 1–21.
20. Ilinca, G. Classic skarn localities of Romania: Contact metamorphism and mineralization related to Late Cretaceous magmatism. *Acta Mineral. Petrogr.* **2010**, *23*, 1–50.
21. Ilinca, G. Upper Cretaceous contact metamorphism and related mineralizations in Romania. *Acta Mineral.-Petr. Abstr. Ser.* **2012**, *7*, 59–64.
22. Neubauer, F. Contrasting Late-Cretaceous with Neogene ore provinces in the Alpine-Balkan-Carpathian-Dinaride collision belt. In *The Timing and Location of Major Ore Deposits in an Evolving Orogen*; Blundell, D., Neubauer, F., von Quadt, A., Eds.; Geological Society (London) Special Publication: London, UK, 2002; Volume 204, pp. 81–102.
23. Săndulescu, M.; Kräutner, H.; Borcoş, M.; Năstăseanu, S.; Patrulius, D.; Ştefănescu, M.; Ghenea, C.; Lupu, M.; Savu, H.; Bercia, I.; et al. *Geological Map of Romania, Scale 1:1,000,000*; Institute of Geology and Geophysics: Bucharest, Romania, 1978.
24. Stoici, S.D. Geological and petrographical study of the upper basin of Crişul Negru—Băiţa Bihor, with special look on the boron mineralization and magnesian skarns. *St. Tehn. Econ. Inst. Geol. Geofiz. Ser. I* **1974**, *7*, 1–198. (In Romanian)
25. Marincea, S. New data on szaibelyite from the type locality, Băiţa Bihor, Romania. *Can. Min.* **2001**, *39*, 111–127.
26. Stoici, S.D. *The Metallogenetic District Băiţa Bihor*; Academiei, Ed.; Bucharest, Romania, 1983; pp. 1–189. (In Romanian)
27. Ştefan, A.; Lazăr, C.; Berbeleac, I.; Udubaşa, G. Evolution of the Banatitic magmatism in the Apuseni Mts. and the associated metallogenesis. *Dări de Seamă ale Sedinţelor Institutului de Geologie şi Geofizică* **1988**, *72–73/2*, 195–213.
28. Pavelescu, L.; Pop, G.O.; Weisz, E.; Popescu, G. La nature et l'âge du batholite banatitique de Bihor. In Proceedings of the 13th Congress of the Carpatho-Balkan Geological Association (KBGA), Cracow, Poland, 5–10 September 1985; Geol. Inst. Ed., Warsaw, pp. 98–101.
29. Bleahu, M.; Soroiu, M.; Catilina, R. On the Cretaceous tectonic-magmatic evolution of the Apuseni Mountains as revealed by K-Ar dating. *Rev. Roum. Phys*. **1984**, *29*, 123–130.
30. Gallhofer, D. *Magmatic Geochemistry and Geochronology in Relation to the Geodynamic and Metallogenetic Evolution of the Banat Region and Apuseni Mountains of Romania*; Diss. ETH no 22888; ETH: Zürich, Switzerland, 2015; pp. 1–145.
31. Bordea, S.; Bleahu, M.; Bordea, I. New stratigraphic and structural data on Western Bihor: The Următ and Vetre Units. *Dări de Seamă ale Şedinţelor Institutului de Geologie şi Geofizică* **1975**, *11*, 61–83. (In Romanian)
32. Gherasi, N. Microfacies, thermal and metasomatic metamorphism in the upper basin of Crişul Negu. *Dări de Seamă ale Şedinţelor Institutului Geologic* **1967**, *54*, 22–54. (In Romanian)
33. Appleman, D.E.; Evans, H.T., Jr. *Indexing and Least-Squares Refinement of Powder Diffraction Data*; U.S. Geological Survey, Computer Contribution 20, (NTIS Doc. PB-216); Springfield, VA, USA, 1973.
34. Benoit, P.H. Adaptation to microcomputer of the Appleman-Evans program for indexing and least-squares refinement of powder-diffraction data for unit-cell dimensions. *Am. Mineral*. **1987**, *72*, 1018–1019.
35. Pouchou, J.L.; Pichoir, F. PAP ϕ (ρZ) procedure for improved quantitative microanalysis. In *Microbeam Analysis*; Armstrong, J.T., Ed.; San Francisco Press: Berkeley, CA, USA, 1985; pp. 104–106.
36. Agilent Technologies. *Xcalibur CCD System, CrysAlis Software System*; Agilent Technologies: Yarnton, Oxfordshire, UK, 2012.
37. Palatinus, L.; Chapuis, G. Superflip—A computer program for the solution of crystal structures by charge flipping in arbitrary dimensions. *J. Appl. Crystallogr.* **2007**, *40*, 786–790.
38. Petříček, V.; Dušek, M.; Palatinus, L. Crystallographic computing system Jana2006: General features. *Z. Kristallogr*. **2014**, *229*, 345–352.
39. Del Valle, C.A. Cristallochimie des Minéraux W-Mo de Skarns de Haute-Température des Monts Banat et Apuseni (Ouest de la Roumanie). Master's Thesis, University of Liège, Liège, Belgium, 2019, pp. 1–93.
40. Droop, G.T.R. A general equation for estimating Fe^{3+} concentrations in ferromagnesian silicates and oxides from microprobe analyses, using stoichiometric criteria. *Mineral. Mag*. **1987**, *51*, 431–435.
41. Long, J.V.P.; Agrell, S.O. The cathode-luminescence of minerals in thin sections. *Min. Mag*. **1965**, *34*, 318–326.
42. Peacock, M.A. On wollastonite and parawollastonite. *Am. J. Sci*. **1935**, *30*, 495–529.
43. Mamedov, K.S.; Belov, N.V. Crystal structure of wollastonite. *Dokl. Akad. Nauk. SSSR* **1956**, *107*, 463–466. (In Russian)

44. Mandarino, J.A. The Gladstone-Dale relationship. IV. The compatibility concept and its application. *Can. Mineral.* **1981**, *19*, 441–450.
45. Buerger, M.J. The arrangement of atoms in crystals of the wollastonite group of metasilicates. *Proc. Nat. Acad. Sci. USA* **1956**, *42*, 113–116.
46. Buerger, M.J.; Prewitt, C.T. The crystal structure of wollastonite and pectolite. *Proc. Nat. Acad. Sci. USA* **1961**, *47*, 1884–1888.
47. Prewitt, C.T. Structure and Crystal Chemistry of Wollastonite and Pectolite. Ph.D. Thesis, Massachusetts Institute of Technology, Cambridge, MA, USA, 1962; 292p.
48. Peacor, D.R.; Prewitt, C.T. Comparison of the crystal structures of bustamite and wollastonite. *Am. Mineral*. **1963**, *48*, 588–596.
49. Prewitt, C.T.; Buerger, M.J. Comparison of the crystal structures of wollastonite and pectolite. *Mineral. Soc. Am. Spec. Papers* **1963**, *1*, 293–302.
50. Ohashi, Y.; Finger, L.W. The role of octahedral cations in pyroxenoid crystal chemistry. I. Bustamite, wollastonite, and the pectolite-schizolite-serandite series. *Am. Mineral*. **1978**, *63*, 274–288.
51. Ohashi, Y. Polysynthetically-twinned structures of enstatite and wollastonite. *Phys. Chem. Miner*. **1984**, *10*, 217–229.
52. Angel, R.J. Structural variation in wollastonite and bustamite. *Mineral. Mag.* **1985**, *49*, 37–48.
53. Mazzucato, E.; Gualtieri, A.F. Wollastonite polytypes in the CaO-SiO_2 system. Part I. Crystallisation kinetics. *Phys. Chem. Miner.* **2000**, *27*, 565–574.
54. Seryotkin, Y.V.; Sokol, E.V.; Kokh, S.N. Natural pseudowollastonite: Crystal structure, associated minerals, and geological context. *Lithos* **2012**, *134–135*, 75–90.
55. Milani, S.; Comboni, D.; Lotti, P.; Fumagalli, P.; Ziberna, L.; Maurice, J.; Hanfland, M.; Merlini, M. Crystal structure evolution of $CaSiO_3$ polymorphs at Earth's mantle pressures. *Minerals* **2021**, *11*, 652.
56. Liebau, F. Über die Kristallstruktur des Pyroxmangits [(Mn, Fe, Ca, Mg)SiO_3]$_x$. *Naturwissenschaften* **1957**, *44*, 178.
57. Ito, T.; Sadanaga, R.; Takeuchi, Y.; Tokonami, M. The existence of partial mirrors in wollastonite. *Proc. Jpn. Acad.* **1969**, *45*, 913–918.
58. Murouchi, Y.; Okuno, M.; Sasaki, N. Amorphization of wollastonite and diopside by ball milling. *Sci. Rep. Kanazawa Univ.* **2021**, *65*, 17–30.
59. Kalinkina, E.V.; Kalinkin, A.M.; Forsling, W.; Makarov, A.M. Sorption of atmospheric carbon dioxide and structural changes of Ca and Mg silicate minerals during grinding. II. Enstatite, åkermanite and wollastonite. *Int. J. Miner. Process.* **2001**, *61*, 289–299.
60. Kubicki, J.D.; Hemley, R.J.; Hofmeister, A.M. Raman and infrared study of pressure-induced structural changes in $MgSiO_3$, $CaMgSi_2O_6$, and $CaSiO_3$ glasses. *Am. Mineral*. **1992**, *77*, 258–269.
61. Park, J.H.; Min, D.J.; Song, H.S. FT-IR spectroscopic study on structure of CaO–SiO_2 and CaO–SiO_2–CaF_2 slags. *ISIJ Int.* **2002**, *42*, 344–351.
62. Khalil, E.M.A.; El Batal, F.H.; Hamdy, Y.M.; Zidan, H.M.; Aziz, M.S.; Abdelghany, A.M. Infrared absorption spectra of transition metals-doped soda lime silica glasses. *Phys. B Condens. Matter* **2010**, *405*, 1294–1300.
63. Lazarev, A.N.; Tenisheva, T.F. Vibrational spectra of silicates III. Infrared spectra of pyroxenoids and other chain metasilicates. *Opt. Spektrosk*. **1961**, *11*, 316–317, 584–587.
64. Rutstein, M.S.; White, W.B. Vibrational spectra of high-calcium pyroxenes and pyroxenoids. *Am. Mineral*. **1971**, *56*, 877–887.
65. Zhao, W.; Zhang, Q.; Peng, C. FTIR spectra for molecular structure of wollastonite. *J. Chin. Ceram. Soc*. **2006**, *34*, 1137–1139.
66. Huang, E.; Chen, C.H.; Huang, T.; Lin, E.H.; Xu, J.-A. Raman spectroscopic characteristics of Mg-Fe-Ca pyroxenes. *Am. Mineral*. **2000**, *85*, 473–479.
67. Buzatu, A.; Buzgar, N. The Raman study of single-chain silicates. *Analele St. Univ. "Al. I. Cuza" Iaşi Geol*. **2010**, *56*, 107–125.
68. Yin, C.D.; Okuno, M.; Morikawa, H.; Marumo, F.; Yamanaka, T. Structural analysis of $CaSiO_3$ glass by X-ray diffraction and Raman spectroscopy. *J. Non-Cryst. Solids* **1986**, *80*, 167–174.
69. Harker, R.T.; Tuttle, O.F. Experimental data on the P_{CO2}—T curve for the reaction: Calcite + quartz = wollastonite + carbon dioxide. *Am. J. Sci*. **1956**, *254*, 239–256.
70. Greenwood, H.J. Wollastonite: Stability in H_2O–CO_2 mixtures and occurrence in a contact—Metamorphic aureole near Salmo, British Columbia, Canada. *Am. Mineral*. **1967**, *52*, 1669–1680.
71. Holland, T.J.B.; Powell, R. An improved and extended internally consistent thermodynamic dataset for phases of petrological interest, involving a new equation of state for solids. *J. Metamorph. Geol*. **2011**, *29*, 333–383.
72. Grammatikopoulos, T.A.; Clark, A.H. A comparative study of wollastonite skarn genesis in the Central Metasedimentary Belt, southeastern Ontario, Canada. *Ore Geol. Rev*. **2006**, *29*, 146–161.

73. Korzhinskii, D.S. *Theory of Metasomatic Zoning*; Agrell, J., Trans.; Clarendon Press: Oxford, UK, 1970; pp. 1–162.
74. Kalinin, D.V. Lower temperature boundaries for the formation of tremolite, diopside and wollastonite under hydrothermal conditions; experimental data. *Geochem. Intern*. **1967**, *4*, 836–839.
75. Jellinek, F.; Brauer, G.; Müller, H. Molybdenum and niobium sulphides. *Nature* **1960**, *185*, 376–377.